



Photoluminescence of InGaN-based red multiple quantum wells

XIN HOU,¹ SHAOSHENG FAN,¹ DAISUKE IIDA,²  YANG MEI,¹ 
BAOPING ZHANG,^{1,*} AND KAZUHIRO OHKAWA² 

¹Laboratory of Micro/Nano-Optoelectronics, Department of Micro Electronic and Integrated Circuits, Xiamen University, Xiamen 361005, China

²Computer, Electrical and Mathematical Sciences and Engineering (CEMSE) Division, King Abdullah University of Science and Technology (KAUST), Thuwal 23955-6900, Saudi Arabia

*bzhang@xmu.edu.cn

Abstract: Optical properties of InGaN-based red LED structure, with a blue pre-well, are reported. Two emission peaks located at 445.1 nm (P_B) and 617.9 nm (P_R) are observed in the PL spectrum, which are induced by a low-In-content blue InGaN single quantum well (SQW) and the red InGaN double quantum wells (DQWs), respectively. The peak shift of P_B with increase of excitation energy is very small, which reflects the built-in electric field of P_B -related InGaN single QW is remarkably decreased, being attributed to the significant reduction of residual stress in the LED structure. On the other hand, the P_R peak showed a larger shift with increase of excitation energy, due to both the screening of built-in electric field and the band filling effect. The electric field in the red wells is caused by the large lattice mismatch between high-In-content red-emitting InGaN and surrounding GaN. In addition, the anomalous temperature dependences of the P_R peak are well elucidated by assuming that the red emission comes from quasi-QD structures with deep localized states. The deep localization suppresses efficiently the escape of carriers and then enhances the emission in the red, leading to high internal quantum efficiency (IQE) of 24.03%.

© 2021 Optical Society of America under the terms of the [OSA Open Access Publishing Agreement](#)

1. Introduction

III-nitride materials are excellent candidates for fabricating visible light-emitting diodes (LEDs), due to the tunable emission band covering from UV to visible wavelength. InGaN-based blue/green LEDs have been commercialized and applied in illumination and displays. The optical properties of InGaN active regions at these wavelengths have also been widely studied. After the commercialization of blue/green LEDs, researches on InGaN-based red LEDs are growing rapidly, because it is essential to realize monolithic integration of full color displays using the same material system. High indium content in the InGaN active layer plays an important role in achieving longer wavelengths emission. However, InGaN layers with a high-In-content have some critical issues, including the significant lattice mismatch [1,2], the strong quantum-confined Stark effect (QCSE) [3,4], phase separation [5,6] and the degradation of crystal quality [7,8]. Therefore, obtaining InGaN active region with high-crystal quality and high-In-content simultaneously is a significant challenge.

In recent years, several methods have been proposed to achieve the III-nitride-based orange, amber and red LEDs, such as utilizing patterned microstructures [7], hybrid multiple quantum wells (MQWs) [9], quantum dot structures [10,11], and strain-engineering methods [12–14]. In 2019, Jiang et al reported the 565 nm yellow LEDs by inserting a pre-strained layer in active region to improve material quality and reduce the compressive strain of InGaN quantum wells [15]. In 2016 and 2020, Iida et al reported the 620 and 633-nm red LEDs [16,17] by decreasing residual in-plane stress in active region and of a hybrid MQWs structure, respectively. However, the emission mechanism related to the red MQWs structures are still not fully studied. A deep

understanding of the emission mechanism as well as the carrier's transmission in InGaN-based red MQWs are important for further development of InGaN-based optoelectronics devices with higher-In-content.

In this paper, we investigate the optical properties of InGaN-based red LED structure, with a blue pre-well, by measuring the excitation energy and temperature dependent photoluminescence (PL) spectra. Two emission peaks locating at 445.1 nm (defined as P_B) and 617.9 nm (defined as P_R) are observed in the PL spectrum. The small shift of P_B with increase of excitation energy reflects the significant reduction of built-in electric field in the InGaN single blue QW. In addition, the anomalous temperature-dependent P_R peak are well elucidated by assuming that the red emission comes from quasi-QD structures with deep localized states. The deep localization centers suppress efficiently the escape of carriers and then enhance the emission in the red.

2. Sample structure and experiments

Figure 1 shows the cross-sectional schematic of the red InGaN LED structure grown on a patterned c-plane sapphire substrate by metalorganic vapor-phase epitaxy (MOVPE). The precursors of Ga, Al, In and N, were trimethylgallium (TMGa), trimethylaluminum (TMAI), trimethylindium (TMIn), and ammonia (NH_3), respectively [17]. The characteristics of the epitaxial structure include a 4- μm thick underlying n-GaN layer, a low-In-content blue InGaN single QW (SQW), and high-In-content red InGaN DQWs. The blue SQW is expected to suppress the strain relaxation and improve the crystalline-quality of red InGaN DQWs [9,18].

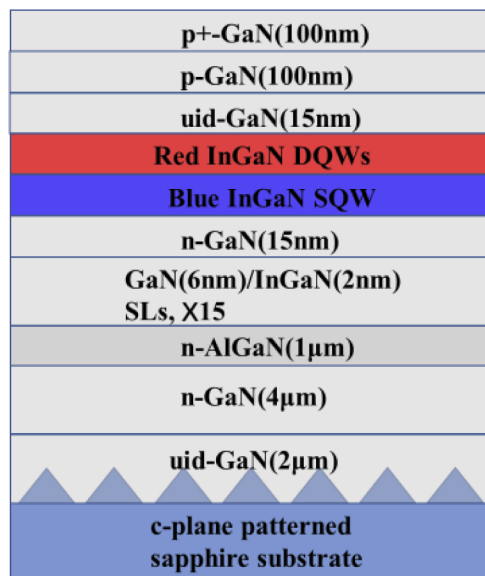


Fig. 1. Cross-sectional schematic of red InGaN-based LED structure

For the temperature-dependent PL measurements, the sample was mounted in a helium closed-circuit cryostat and the temperature was controlled from 4 to 300 K. A 405 nm laser with 5 ns pulse duration and 20 Hz repeat frequency was used as excitation source. The PL signal from the sample was dispersed by a Princeton instruments ACTONSpectrapro-3000i monochromator and detected by a thermoelectrically cooled Synapse CCD detector.

3. Experimental results and discussion

Figure 2 shows the normalized PL spectra under varying excitation energy at low temperature (4 K). Two peaks with emission wavelengths of 445.1 nm (P_B) and 617.9 nm (P_R) are clearly observed. The P_R exhibited a wider full-width at half-maximum (FWHM) which is attributed to the inhomogeneity of In-content in the red QWs. The P_R and P_B both show a blue shift in peak wavelength with increasing excitation energy. The corresponding mechanisms, however, are different. Usually, screening of built-in electric field and band-filling account for the blue shift. The blue shift of P_B is mainly characterized by the broadening at the high energy part of the peak, demonstrating the domination of band-filling effect. In other words, the built-in electric field of the blue SQW is significantly reduced, due to the thinner (~ 2 nm) SQW [17] and the underlying n-type strain-modulation structure composed by n-GaN, n-AlGaIn and n-SLs [19]. On the other hand, P_R shows a blue shift of the entire peak at lower excitation densities, and a further broadening at higher excitations. This indicates the variation from screening of QCSE (or electric field) to band-filling. The appearance of QCSE is attributed to the large lattice mismatch between high-In-content red-emitting InGaIn and surrounding GaIn. In detail, a blue shift of 28.7 nm was observed in P_R with the increase in excitation energy from 0.06 μJ to 6 μJ , which caused by the large QCSE in red DQWs. When the excitation energy exceeds beyond 4 μJ , the broadening at the shorter wavelength side of the spectra can be attributed to the evident band-filling effect. The P_R exhibits a noticeable blue shift and strong luminescence at the low energy peak, showing the characteristics of strongly localized states. According to the above analysis and previous reported literatures [20,21], the two emission peaks are assigned to the blue InGaIn single QW (445.1 nm) and the high-In-content quasi-QD (617.9 nm) in red InGaIn DQWs [16]. The power densities of different excitation energies are calculated as shown in Table 1.

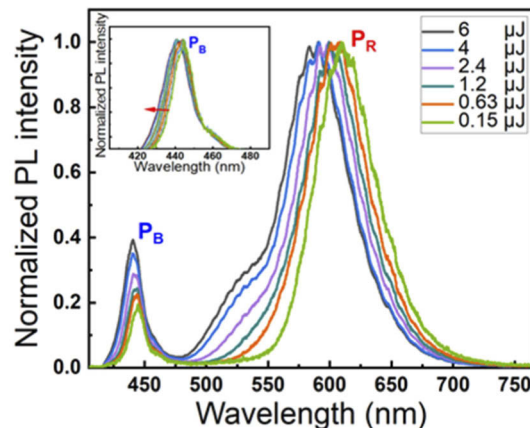


Fig. 2. Normalized PL spectra with different excitation energy at low temperature (4 K); the inset shows normalized PL spectra of P_B peak.

Table 1. The power densities of different excitation energies

Excitation energy (μJ)	0.15	0.63	1.20	2.40	4.00	6.00
Power density (KW/cm^2)	149.3	626.9	1194	2388	3981	5971

The peak energy and FWHM of P_R and P_B as a function of the excitation energy are shown in Fig. 3. Gaussian fitting is used to fit the curves of the two emission peaks so as to obtain the peak positions and FWHMs. Due to the higher In-content of red DQWs, the energy value of P_R is lower than that of P_B . Meanwhile, the In-content fluctuation in quasi-QD leads to the

broadening of FWHM. The peak energy and FWHM of P_R increase about 97.89 meV and 7.46 nm, respectively, monotonically with increasing excitation energy, whereas for P_B corresponding values are 27.97 meV and 5.27 nm. The total blue-shift of peak positions for the P_R emission is more obvious than that for the P_B in the range of excitation energies. The significant band-filling effect indicates the carriers in active region are hardly to be captured by the non-radiative recombination centers at 4 K [22]. The photo-generated carriers are easily transferred to the localized centers of high-In-content quasi-QDs and the low-In-content blue SQW [17].

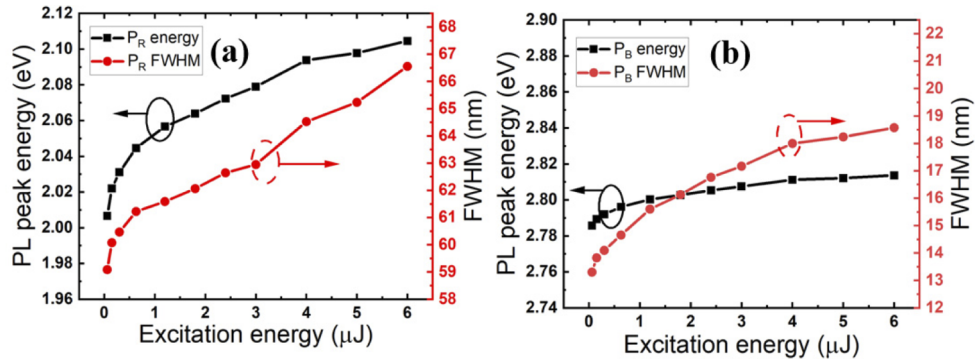


Fig. 3. Emission peak energy and full width at half maximum (FWHM) as functions of excitation energy for the red LED structure at 4 K, (a) P_R and (b) P_B .

For further investigation, the temperature dependencies of peak energy and FWHM were measured at an excitation energy of $3\mu\text{J}$. The temperature behavior of P_R is illustrated in Fig. 4(a). Under the excitation energy of $3\mu\text{J}$, the band-filling effect is more remarkable than the Coulomb screening effect of QCSE in quasi-QD. The peak energy and FWHM of P_R show a monotonically increase up to room temperature. The absence of the S-shaped temperature-dependent behavior, which is typically observed in InGaN QWs, indicated the strong localization effect of carriers, which are originated from the quasi-QDs in red QWs with high In-content [22]. This is due to the fact that the confinement energy of quasi-QDs is very large so that the thermal activation cannot make the carriers escape from the quasi-QDs. Consequently, the red shift was not observed in our experiment. The deep localization helps to enhance the radiative recombination efficiency of red quasi-QDs. In contrast, the temperature dependent peak energy of P_B is a typical S-shaped curve (slightly redshift-blueshift-redshift), as shown in Fig. 4(b). At lower temperature, the almost no shift of P_B is observed with rise of temperature, indicating the homogeneous In-content of the blue SQW. At higher temperature, the P_B energy decreases markedly up to 300 K, in agreement with the temperature-induced band-gap shrinkage [23].

In order to investigate the properties of the different localization centers, one-channel Arrhenius model is used to analyze the temperature-dependent PL of the two peaks.

$$I(T) = \frac{I_0}{\left[1 + A \cdot \exp\left(-\frac{E_a}{k_B T}\right)\right]}$$

where I_0 is the integrated PL intensity at low temperature, A is the constant related to the density of the localization states, E_a is the activation energy of the corresponding nonradiative centers induced by defects and k_B is the Boltzmann constant. The fitting results of two emission peaks obtained from this model are shown in Fig. 5.

At lower temperature, the non-radiative recombination centers are frozen and inactivated. The carriers are easily captured and restricted by the localized states. Contrastively, at higher temperature, the carriers in localized states and non-radiative centers are thermally activated. The

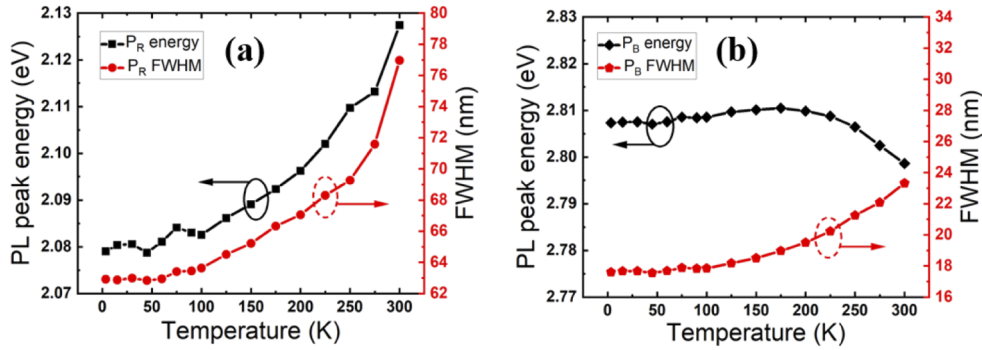


Fig. 4. Temperature dependence of PL peaks energies and FWHM measured at excitation energy $3\mu\text{J}$, (a) P_R and (b) P_B .

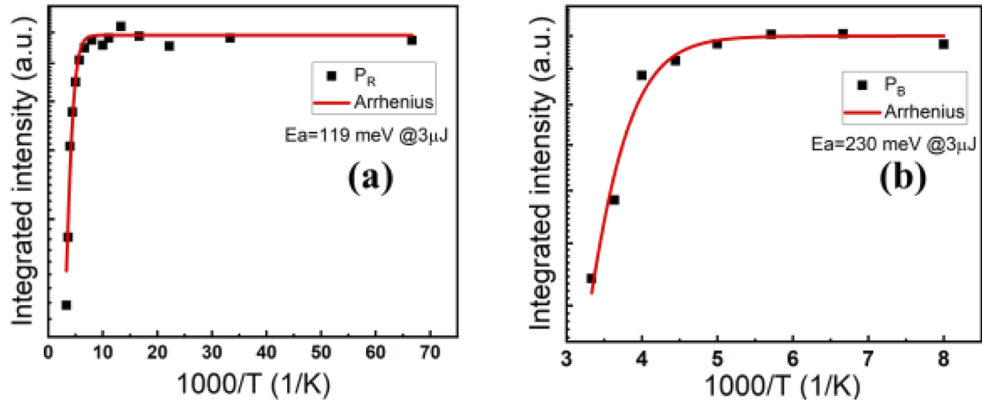


Fig. 5. Arrhenius plots of PL intensity versus temperature of (a) P_R and (b) P_B .

thermally activated carriers can be trapped by the nonradiative centers, forming the non-radiative recombination process. The values of E_a for P_B and P_R turned out to be 230 and 119 meV, respectively. The activation energy of P_B is much larger than P_R , demonstrating that the density of non-radiative centers in the blue single QW is much less than that of quasi-QDs in red DQWs. It is attributed to the large lattice mismatch between high-In-content red-emitting InGa_N and surrounding GaN.

Figure 6 shows the internal quantum efficiency (IQE) of two emission peaks as functions of the excitation energy. In this work, IQE is defined as the ratio of the integrated PL intensity at 300 K and 15 K. The IQE of P_R increases monotonously with increasing excitation energy. During the increase of excitation energy, the non-radiative centers in the deep localized states are saturated. Meanwhile, the QCSE is screened by the increasing carrier density, enhancing the overlap of electron-hole wavefunction. Therefore, the main recombination process of carriers in quasi-QDs is changed from non-radiative to radiative recombination [24]. The IQE of P_R is increased to 24.03% at the excitation energy of $6\mu\text{J}$. On the contrary, the IQE of P_B is sharply decreased with increasing the excitation energy. Due to the small width and low-In-content of the blue SQW, the carrier confinement is relatively weak. At room temperature, the activated carriers in the blue SQW are easily escaped, which leads to the IQE reduction. With increasing excitation power density, the Auger recombination gradually becomes important too [25]. Thus, the IQE of blue emission peak decreases monotonously with the increase of excitation energy. In addition, defects may play a role too. At low carrier density, the effect of defects is significant.

At higher carrier density, defects are saturated and their influence becomes less. The IQE of P_B is then decreased to 52.68%. Overall, the IQE of P_B is still higher than P_R . There are two main reasons: first, the high indium content of P_R leads to an increase in the compressive strain at the interface between the InGaN well and the GaN barrier, resulting in the quantum-confined Stark effect (QCSE). Second, a large lattice mismatch exists between high-In-content red-emitting InGaN and surrounding GaN, leading to a large number of defects in red DQWs.

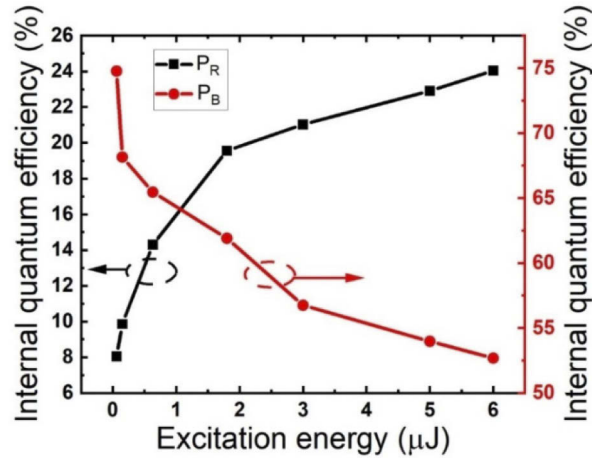


Fig. 6. Internal quantum efficiency of two emission peaks as functions of the excitation energy.

4. Conclusion

In summary, the optical properties of InGaN-based red LED structure was studied by photoluminescence. Two emission peaks, located at 445.1 nm and 617.9 nm, are caused by a low-In-content blue InGaN SQW and the red InGaN DQWs, respectively. The slight shift of P_B with increasing excitation energy reflects that the built-in electric field of P_B -related InGaN SQW was reduced significantly. In contrast, a larger shift of P_R peak with increase of excitation energy is attributed to the screening of built-in electric field and band filling in quasi-QD structures. The built-in electric field should be caused by the large lattice mismatch between high-In-content red-emitting InGaN and surrounding GaN. The deep localization of quasi-QD structures suppresses efficiently the escape of carriers and then enhances the emission in the red, which is the reason for strong emission intensity. The variation of internal quantum efficiency with excitation intensities indicates the better crystal quality of blue pre-well and the occurrence of defects in the red-emitting structures. The experimental results will provide a useful guidance to fabricate a longer wavelength InGaN-based optoelectronic devices with high-quantum efficiency.

Funding. National Key Research and Development Program of China (2017YFE0131500).

Acknowledgments. The authors would like to thank Zhong-Ming Zheng, Huan Xu, Lei-Ying Ying, Zhi-Wei Zheng and Hao Long of Xiamen University for support and useful discussions.

Disclosures. The authors declare no conflicts of interest.

Data availability. Data underlying the results presented in this paper are not publicly available at this time but may be obtained from the authors upon reasonable request.

References

1. T. Taki, H. Seki, N. Takahashi, and A. Koukitu, "Thermodynamic analysis of the MOVPE growth of $\text{In}_x\text{Ga}_{1-x}\text{N}$," *J. Cryst. Growth* **170**(1-4), 306–311 (1997).
2. Yamashita Youji, Tamura Hitoshi, and Naohika and Horio, "Control of emission wavelength of GaInN single quantum well, light emitting diodes grown by metalorganic chemical vapor deposition in a split-flow reactor," *Jpn. J. Appl. Phys.* **42**(Part 1, No. 7A), 4197–4202 (2003).
3. M. Shimizu, Y. Kawaguchi, K. Hiramatsu, and N. Sawaki, "Metalorganic vapor phase epitaxy of thick InGaN on sapphire substrate," *Jpn. J. Appl. Phys.* **36**(Part 1, No. 6A), 3381–3384 (1997).
4. D. Holec, P. Costa, M. J. Kappers, and C. J. Humphreys, "Critical thickness calculations for InGaN/GaN," *J. Cryst. Growth* **303**(1), 314–317 (2007).
5. D. Iida, Z. Zhuang, P. Kirilenko, M. Velazquez-Rizo, and K. Ohkawa, "High-color-rendering-index phosphor-free InGaN-based white light-emitting diodes by carrier injection enhancement via v-pits," *Appl. Phys. Lett.* **117**(17), 172103 (2020).
6. T. Mukai, M. Yamada, and S. Nakamura, "Characteristics of InGaN-based uv/blue/green/amber/red light-emitting diodes," *Jpn. J. Appl. Phys.* **38**(Part 1, No. 7A), 3976–3981 (1999).
7. R. Hashimoto, J. Hwang, S. Saito, and S. Nunoue, "High-efficiency green-yellow light-emitting diodes grown on sapphire (0001) substrates," *Phys. Sta. Sol. C* **10**(11), 1529–1532 (2013).
8. Y. Zhao, H. O. Sang, W. Feng, Y. Kawaguchi, S. Tanaka, and K. Fujito, "Green semipolar (2021) InGaN light-emitting diodes with small wavelength shift and narrow spectral linewidth," *Appl. Phys. Express* **6**(6), 062102 (2013).
9. D. Iida, S. Lu, S. Hirahara, K. Niwa, and K. Ohkawa, "Enhanced light output power of InGaN-based amber LEDs by strain-compensating AlN/AlGaIn barriers," *J. Cryst. Growth* **448**, 105–108 (2016).
10. G. E. Weng, W. R. Zhao, S. Q. Chen, H. Akiyama, Z. C. Li, and J. P. Liu, "Strong localization effect and carrier relaxation dynamics in self-assembled InGaN quantum dots emitting in the green," *Nano Lett.* **10**(1), 1–7 (2015).
11. Y. Mei, G. E. Weng, B. P. Zhang, J. P. Liu, W. Hofmann, L. Y. Ying, J. Y. Zhang, Z. C. Li, H. Yang, and H. C. Kuo, "Quantum dot vertical-cavity surface-emitting lasers covering the 'green gap'," *Light Sci Appl* **6**(1), e16199 (2017).
12. D. Iida, Z. Zhuang, P. Kirilenko, M. Velazquezrizo, and K. Ohkawa, "Demonstration of low forward voltage InGaN-based red LEDs," *Appl. Phys. Express* **13**(3), 031001 (2020).
13. Y. R. Wu, C. Chiu, C. Y. Chang, P. Yu, and H. C. Kuo, "Size-dependent strain relaxation and optical characteristics of InGaIn/GaN nanorod LEDs," *IEEE J. Sel. Top. Quantum Electron.* **15**(4), 1226–1233 (2009).
14. C. Y. Wang, L. Y. Chen, C. P. Chen, Y. W. Cheng, and J. J. Huang, "GaN nanorod light emitting diode arrays with a nearly constant electroluminescent peak wavelength," *Opt. Express* **16**(14), 10549–10556 (2008).
15. F. Jiang, J. Zhang, L. Xu, J. Ding, G. Wang, and X. Wu, "Efficient InGaIn-based yellow-light-emitting diodes," *Photonics Res.* **7**(2), 144 (2019).
16. D. Iida, K. Niwa, S. Kamiyama, and K. Ohkawa, "Demonstration of InGaIn-based orange LEDs with hybrid multiple-quantum-wells structure," *Appl. Phys. Express* **9**(11), 111003 (2016).
17. D. Iida, Z. Zhuang, P. Kirilenko, M. Velazquez-Rizo, and K. Ohkawa, "633-nm InGaIn-based red LEDs grown on thick underlying GaN layers with reduced in-plane residual stress," *Appl. Phys. Lett.* **116**(16), 162101 (2020).
18. W. Yao, L. Wang, Y. Meng, S. Yang, X. Liu, and H. Niu, "Stress engineering for reducing the injection current induced blue shift in InGaIn-based red light-emitting diodes," *CrystEngComm* **23**(12), 2360–2366 (2021).
19. K. Lekhal, B. Damilano, H. T. Ngo, D. Rosales, P. D. Mierry, S. Hussain, P. Vennéguès, and B. Gil, "Strain-compensated (Ga,In)N/(Al,Ga)N/GaN multiple quantum wells for improved yellow/amber light emission," *Appl. Phys. Lett.* **106**(14), 160 (2015).
20. Q. Wang, Z. W. Ji, F. Wang, Q. Mou, Y. J. Zheng, X. G. Xu, Y. J. Lü, and Z. H. Feng, "Influence of excitation power on temperature-dependent photoluminescence of phase-separated InGaIn quantum wells," *Chin. Opt. Lett.* **14**(4), 237–241 (2015).
21. R. B. Xu, Y. Mei, B. P. Zhang, L. Y. Ying, Z. W. Zheng, W. Hofmann, J. P. Liu, H. Yang, M. Li, and J. Zhang, "Simultaneous blue and green lasing of GaIn-based vertical-cavity surface-emitting lasers," *Semicond. Sci. Technol.* **32**(10), 105012.1 (2017).
22. H. N. Wang, Z. W. Ji, S. Qu, G. Wang, Y. Z. Jiang, B. L. Liu, X. G. Xu, and H. Mino, "Influence of excitation power and temperature on photoluminescence in InGaIn/GaN multiple quantum wells," *Opt. Express* **20**(4), 3932–3940 (2012).
23. W. Zhao, G. E. Weng, M. Liang, Z. Li, J. P. Liu, J. Zhang, and B. P. Zhang, "Temperature Dependence of Emission Properties of Self-Assembled InGaIn Quantum Dots," *Chin. Phys. Lett.* **613**(114205), 1–4 (2014).
24. Z.-M. Zheng, Y. Mei, H. Long, J. Hoo, S.-P. Guo, Q. X. Li, L. Y. Ying, Z. W. Zheng, and B. P. Zhang, "AlGaIn-Based Deep Ultraviolet Vertical-Cavity Surface-Emitting Laser," *IEEE Electron Device Lett.* **42**(3), 375–378 (2021).
25. X. Zhang, Y. Li, Z. Li, Z. Miao, and J. Li, "Size-Dependent Quantum Efficiency of Flip-Chip Light-Emitting Diodes at High Current Injection Conditions," *Photonics* **8**(4), 88 (2021).